Supplementary Information

May 15, 2024

Performance Parameters of Infra-red and Visible-active MXene Photocatalysts for Water Splitting

Swati Shaw*[a] and Subhradip Ghosh*[b]

[a] *Department of Physics, Indian Institute of Technology Guwahati, Guwahati-781039, Assam, India. E-mail: swatishaw@iitg.ac.in*

[b] *Department of Physics, Indian Institute of Technology Guwahati, Guwahati-781039, Assam, India. E-mail: subhra@iitg.ac.in*

S1 Mechanical properties of M_2COT and $MM'CO_2$ Janus MXenes; M, M′=Sc, Ti, Zr, Hf; T= S, Se

The equilibrium lattice constants, elastic stiffness constants C_{ij}, Young's Modulus, and Poisson ratio of 14 Janus MXenes have been calculated and presented in Table S1. The results suggest that all Janus MXene materials satisfy Born-Huang's criteria and are mechanically stable at their equilibrium volumes. In the M_2COT series, C_{11} gradually increases as M changes from Sc to Hf. This happens due to the gradual increase in mass of the transition metal. The same trend is observed for compounds of $MM'CO_2$ series. Young's Modulus (Y) and Poisson Ratio (ν) stand for the stiffness and mechanical flexibility of a material, respectively. The calculated Y of each M_2COS is larger than that of M_2COSe.This is due to the larger bond lengths of M-Se pairs than that of M-S pairs. Weaker M-Se bonds with respect to M-S bonds are responsible for this trend. For the same reason, ν of M_2COSe are greater than those of M_2COS, signifying greater flexibility of M_2COSe MXenes. Among the compounds of $MM'CO_2$ (M/M′= Ti, Zr, Hf) series, $ZrHfCO_2$ has the heightest Y implying mechanically stability at a higher strain in comparison with $TiZrCO_2$ & $TiHfCO_2$. For the same reason, $ScZrCO_2$ & $ScHfCO_2$ can have mechanical stability at higher strain in comparison with $ScTiCO_2$.

Table S1 The lattice parameter ($a=b$), Elastic Constants (C_{ij}), Young's Modulus (Y) & Poisson Ratio (ν) of 14 Janus MXenes considered.

Compounds	$a=b$ (Å)	C_{11} (Nm^{-1})	C_{22} (Nm^{-1})	C_{12} (Nm^{-1})	C_{66} (Nm^{-1})	Y (Nm^{-1})	ν
Sc_2COS	3.63	123.96	123.78	76.73	23.57	76.34	0.62
Sc_2COSe	3.66	120.76	120.76	72.26	24.25	77.52	0.60
Ti_2COS	3.11	177.48	177.48	64.10	56.69	154.33	0.36
Ti_2COSe	3.12	157.79	157.79	99.82	28.99	94.65	0.63
Zr_2COS	3.39	212.21	212.06	63.18	74.47	193.31	0.30
Zr_2COSe	3.38	199.49	199.49	64.96	67.26	178.34	0.33
Hf_2COS	3.34	234.77	234.49	59.68	87.48	219.45	0.25
Hf_2COSe	3.34	223.32	223.32	62.53	80.40	205.81	0.28
$ScTiCO_2$	3.15	161.15	161.15	75.84	42.66	125.47	0.47
$ScZrCO_2$	3.30	181.24	181.24	79.16	51.04	146.67	0.44
$ScHfCO_2$	3.27	176.83	176.83	78.69	49.07	141.81	0.45
$TiZrCO_2$	3.19	249.51	248.35	91.50	78.71	215.29	0.37
$TiHfCO_2$	3.16	265.00	263.45	89.61	87.31	233.83	0.34
$ZrHfCO_2$	3.29	278.05	277.92	78.34	99.83	255.91	0.28

S2 Dynamical and thermal stability of M_2COT and $MM'CO_2$ Janus MXenes; M, M′=Sc, Ti, Zr, Hf; T= S, Se

Figures (S1)-(S3) show results of phonon dispersion relations for 14 Janus MXenes considered in this work at various bi-axial strains along with variations of their Free energies and temperatures with time when the systems are subjected to the highest strain where they are dynamically stable. We find that most systems are dynamically stable up to 4% of tensile strain. At the highest strain for sustenance of dynamical stability, all compounds are thermally stable at room temperature.

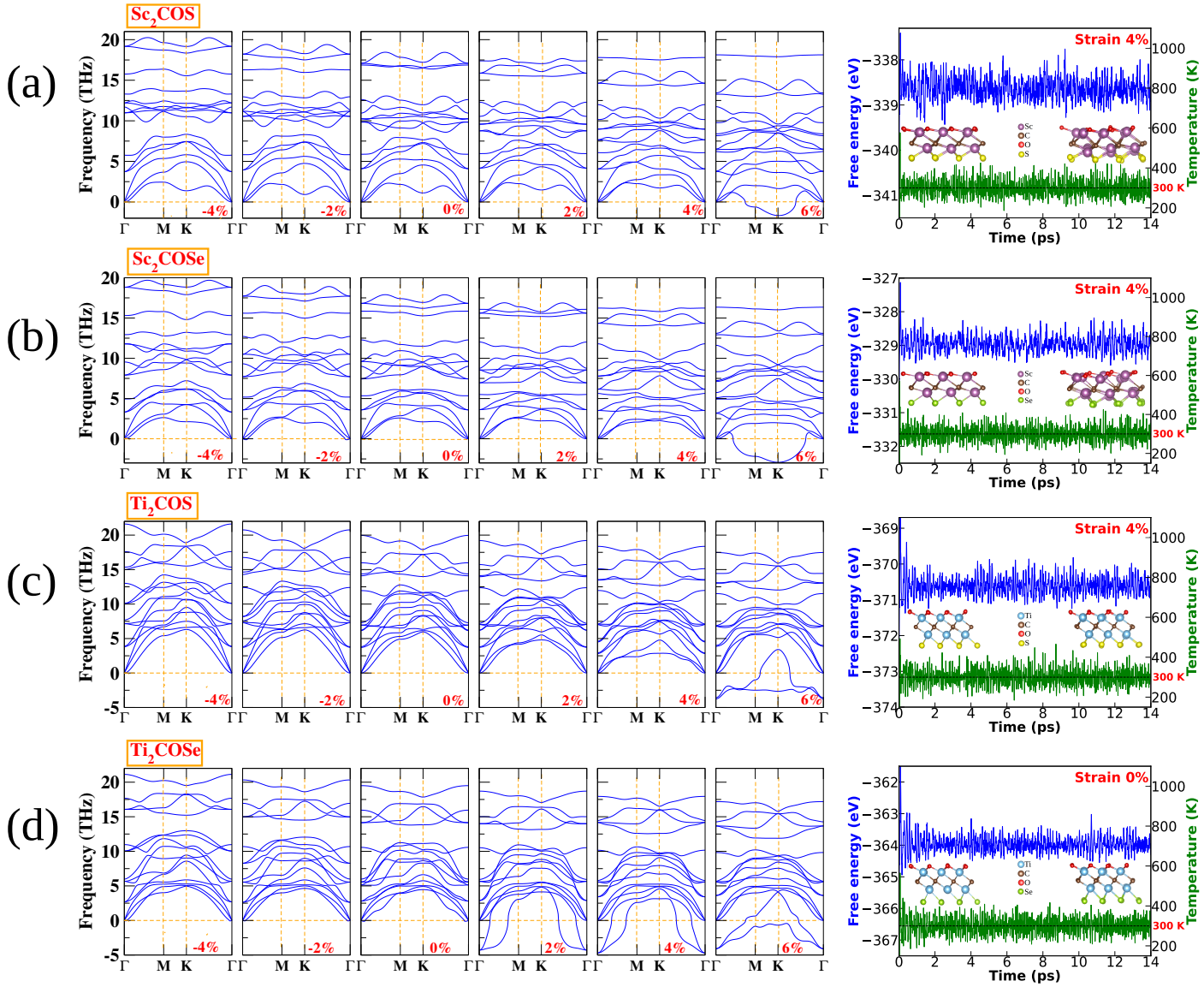

Fig. S1 Phonon dispersion curves of M_2COT (M =Sc, Ti; T=S, Se) MXenes under -2% to 6% Biaxial strains. Variations in free energy and temperature with respect to AIMD simulation time for the systems at maximum possible strains where they are dynamically stable are shown in the rightmost panels of (a)-(d). The initial and final structures (at 300K) are also shown.

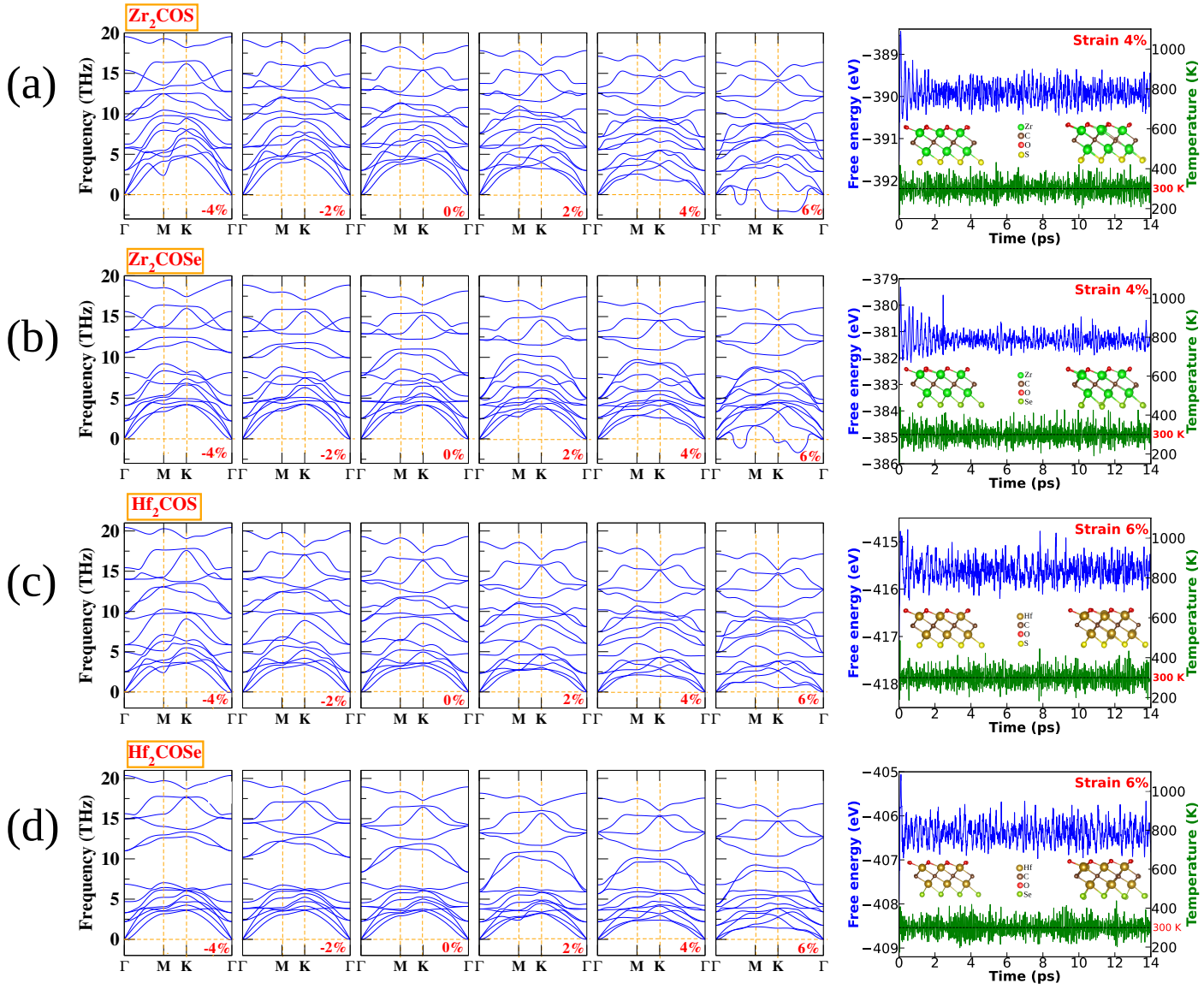

Fig. S2 Phonon dispersion curves of M_2COT (M =Zr, Hf; T=S, Se) MXenes under -2% to 6% Biaxial strains.Variations in free energy and temperature with respect to AIMD simulation time for the systems at maximum possible strains where they are dynamically stable are shown in the rightmost panels of (a)-(d). The initial and final structures (at 300K) are also shown.

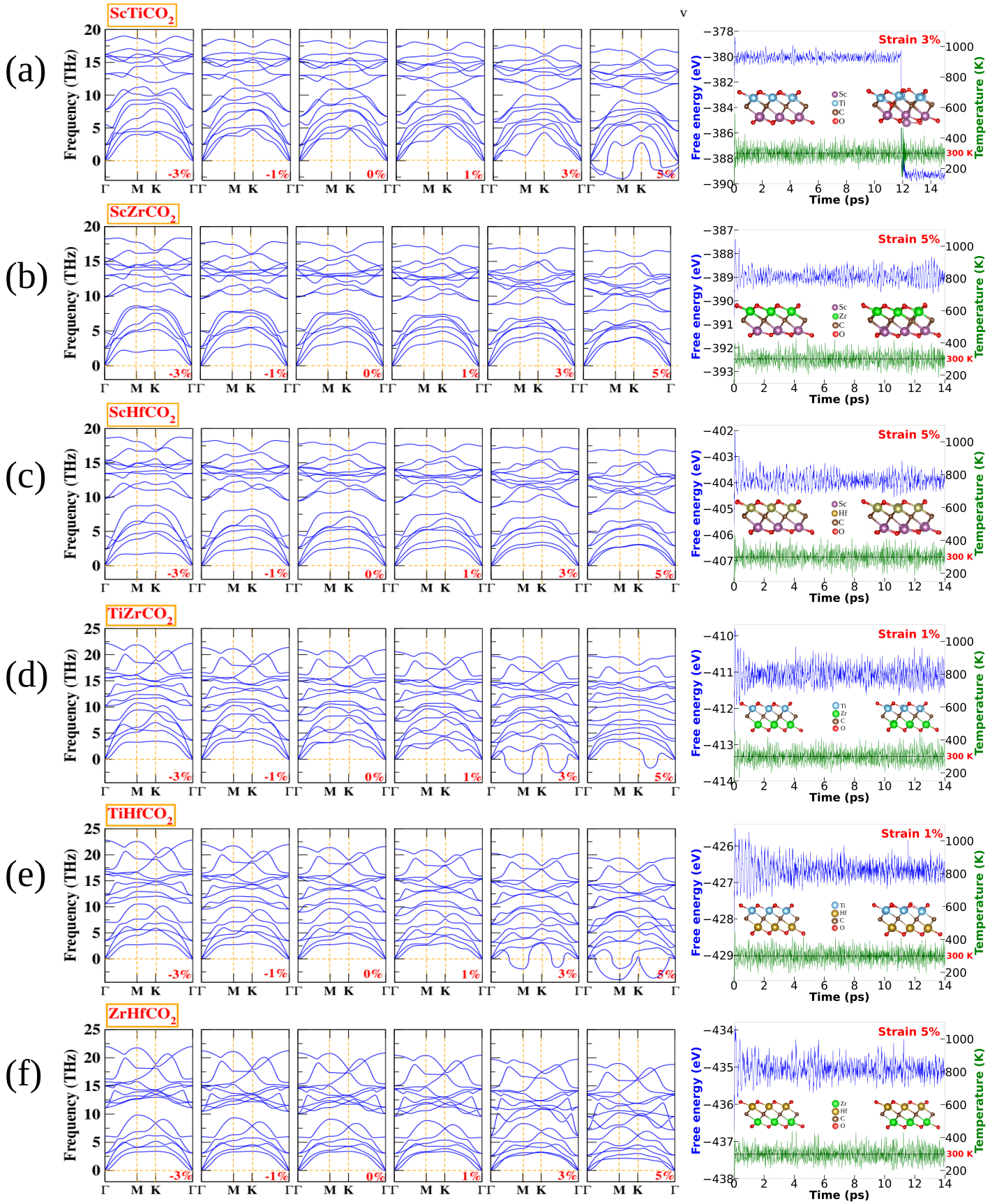

Fig. S3 Phonon dispersion curves of $MM'CO_2$ ((M, M'=Sc, Ti, Zr, Hf) MXenes under -3% to 5% Biaxial strains.Variations in free energy and temperature with respect to AIMD simulation time for the systems at maximum possible strains where they are dynamically stable are shown in the rightmost panels of (a)-(f). The initial and final structures (at 300K) are also shown.

S3 Electronic Band Structures of seven Janus MXenes under Bi-axial strain

In Figure S4, we present the band structures of seven Janus compounds as a function of compressive and tensile strains. These compounds are semiconductors at their equilibrium volumes. We find that baring Zr_2COS and Hf_2COS at 4% compressive strain, all compounds remain semiconductors.

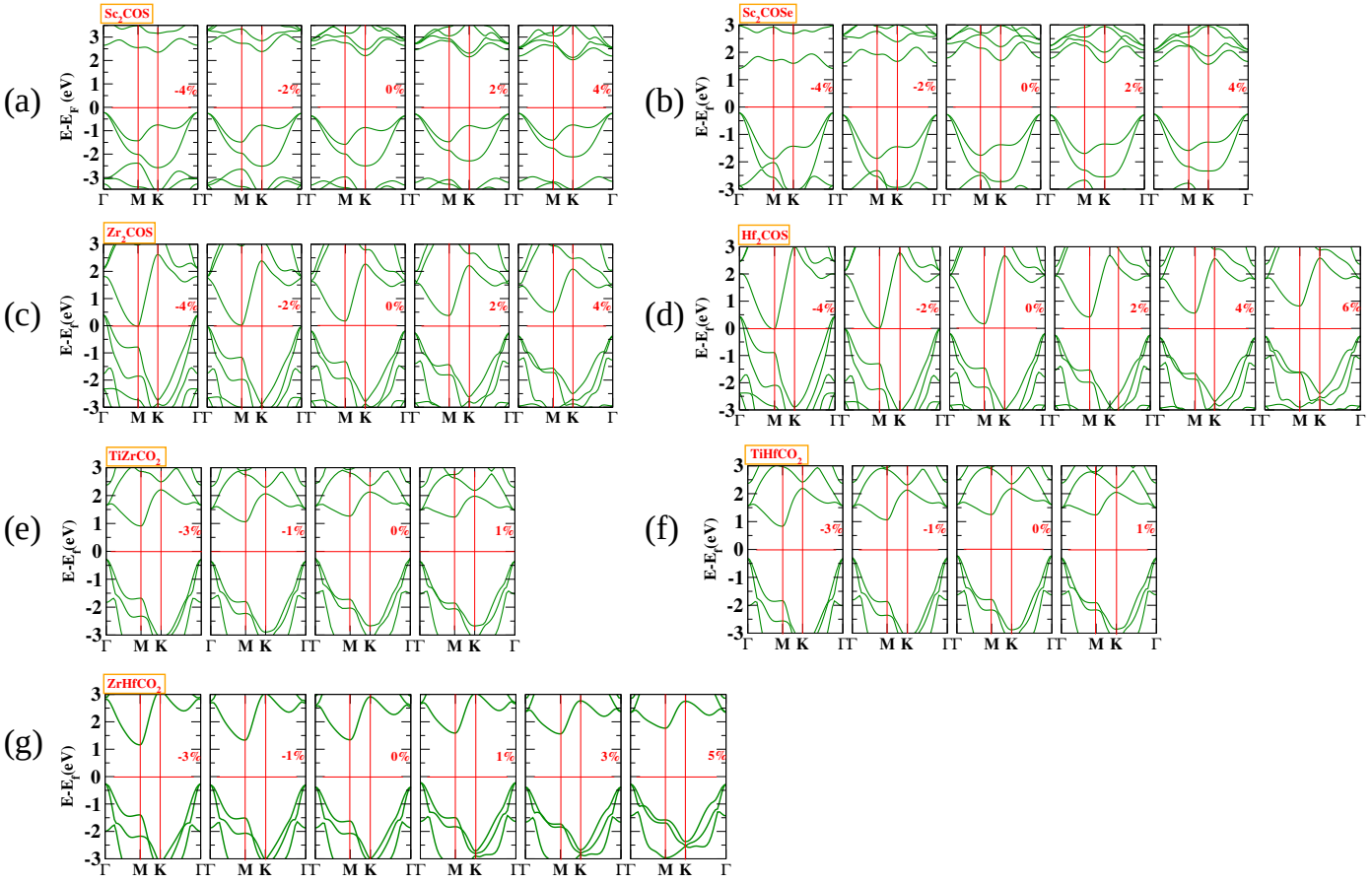

Fig. S4 Electronic Band Structures of a) Sc_2COS, b) Sc_2COSe, c) Zr_2COS, d) Hf_2COS, e) $TiZrCO_2$, f) $TiHfCO_2$ and g) $ZrHfCO_2$ under various Biaxial strains. The Fermi level in each case is marked with a horizontal red line.

S4 Electrostatic potential profile of six Janus MXenes as a function of strain

In Figure S5, variations in the electrostatic potentials across the surfaces of six M_2COT Janus MXenes are presented. The large electronegativity difference between O and T in these compounds induces an internal electric field, causing a potential difference across the surfaces. We find that the potential difference increases with strain. Significant changes are observed in Sc-based compounds and in Hf_2COSe.

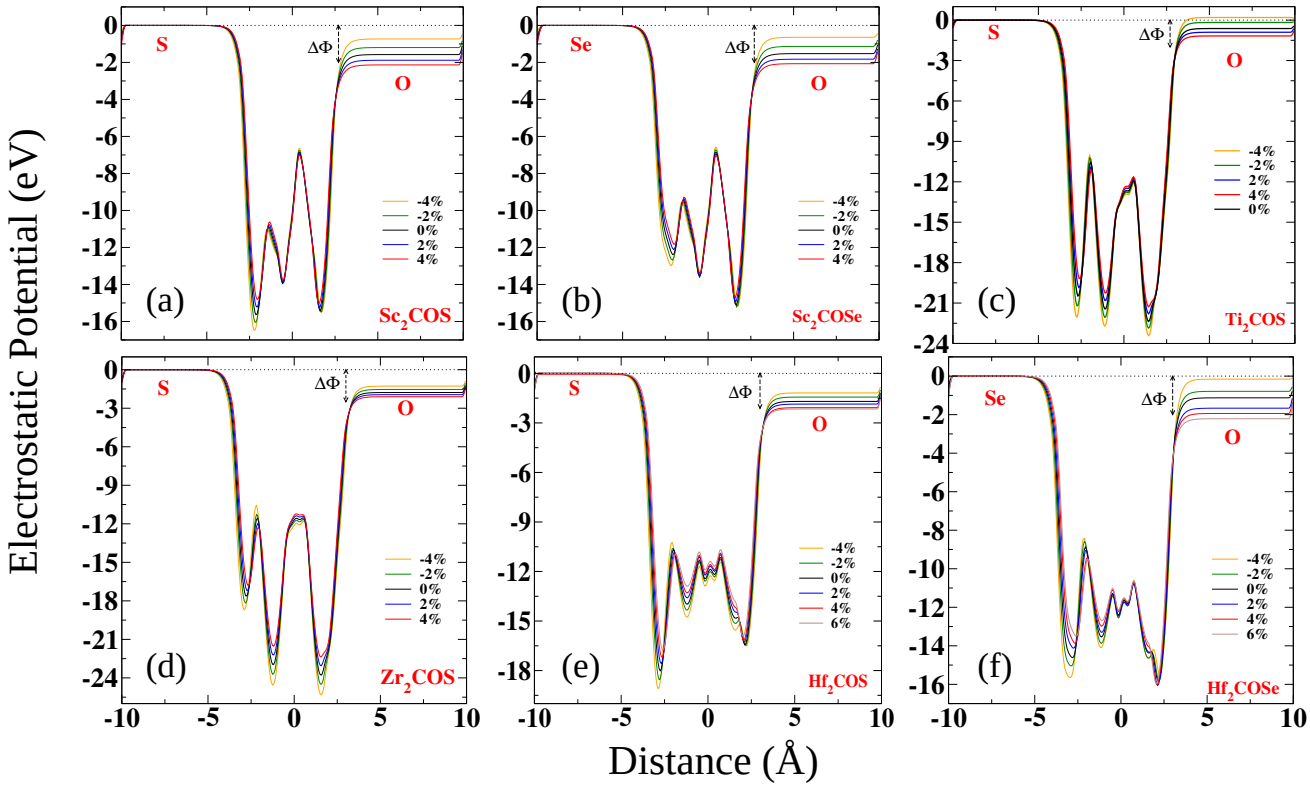

Fig. S5 Variation in electrostatic potential profiles of a) Sc_2COS, b) Sc_2COSe, c) Ti_2COS, d) Zr_2COS, e) Hf_2COS & f) Hf_2COSe with Biaxial strain. Calculations are done by setting the vacuum level of (00-1) surface to zero eV.